Journal of
Materials Chemistry A

ROYAL SOCIETY
OF CHEMISTRY

COMMUNICATION

View Article Online
View Journal | View Issue

Check for updates

Cite this: *J. Mater. Chem. A*, 2024, **12**, 2673

Received 31st July 2023
Accepted 21st November 2023

DOI: 10.1039/d3ta04529c

rsc.li/materials-a

Efficiency enhancement and doping type inversion in Cu_2CdSnS_4 solar cells by Ag substitution†

Ahmad Ibrahim,[a] Stener Lie,[ab] Joel Ming Rui Tan,[ab] Ryan Swope,[c] Axel Gon Medaille,[def] Shreyash Hadke,[c] Edgardo Saucedo,[ef] Rakesh Agrawal[c] and Lydia Helena Wong*[abg]

The main limiting factor of kesterite-related solar cells is the low open-circuit voltage (V_{OC}) relative to their bandgap. This drawback has been correlated with the easily formed anti-site defects caused by similar ionic radii and/or chemical valence. Recent success in suppressing Sn-related defects by using Cd to replace Zn in Cu_2CdSnS_4 was attributed to the higher formation energy of the $2Cu_{Cd}$ + Sn_{Cd} defect complex compared to its counterpart in Cu_2ZnSnS_4. This has motivated the use of bigger ions to replace Cu in Cu_2CdSnS_4 to reduce the possibilities of I_{II} and II_I defect formation. In this work, we substitute Cu in Cu_2CdSnS_4 with larger Ag at various concentrations and investigate the structural, optoelectronic, and photovoltaic properties of $(Cu,Ag)_2CdSnS_4$. Higher concentrations of Ag lead to peak splitting in XRD spectra, which is attributed to mixed phases and marks the transition towards Ag_2CdSnS_4. This is also complemented by Raman scattering analysis, the first time the Raman spectrum of Ag_2CdSnS_4 is reported. Doping type inversion was observed for pure n-type Ag_2CdSnS_4 instead of the p-type of Cu_2CdSnS_4, accompanied by high carrier mobility and sharp absorption onset. Further optoelectronic and photovoltaic characterization reveals that adding 5% Ag concentration improves Cu_2CdSnS_4 device performance to 7.72%, mainly due to superior film quality and improved interface properties. As a result, better carrier collection contributes to the short-circuit current improvement of the champion device.

Introduction

The motivation to address anti-site defects in Cu_2ZnSnS_4 has led to investigations on I_2–II–IV–VI_4 compounds as better solar harvesting materials.[1,2] Anti-site defects in Cu_2ZnSnS_4 occur when one cation replaces another with similar or different oxidation states, resulting in point defects such as Cu_{Zn}, or defect clusters such as $2Cu_{Zn} + Sn_{Zn}$. To mitigate the formation of these defects, cations with larger ionic size differences are utilized to substitute one or more cations with similar ionic sizes, such as Cu or Zn.[3]

Cation substitution in Cu_2ZnSnS_4 is a crucial strategy in further improving its performance. The cation substitution on Cu_2ZnSnS_4 involving the Ag & Cd reduces the V_{OC} deficit caused by both radiative and nonradiative recombination. Partial Cd-alloying of Cu_2ZnSnS_4 has positively impacted grain quality,[4] band alignment,[5] and bandgap fluctuations.[6] As indicated by lower bandgap fluctuation, Cd substitution limits the sub-bandgap absorption compared to Cu_2ZnSnS_4 and elevates the valence band maximum (VBM), improving the band alignment.[6,7] Similarly, Ag substitution has a positive effect, as indicated by lower Urbach energy and reduced anti-site defects.[8] Furthermore, the co-substitution of Ag and Cd on Cu_2ZnSnS_4 improved device efficiency to 10.2%.[9]

Full cation substitution of Cu_2ZnSnS_4 leading to I_2–II–IV–VI_4 compounds has also been explored to pursue different structural and electronic properties. The lack of Cu vacancy in $Ag_2ZnSn(S,Se)_4$ and Zn-rich condition was found to be favorable for forming n-type instead of p-type material.[10] Consequently, a different device configuration needs to be employed.[11,12] CXTS compounds (where X = Mg, Mn, Ni, Co, Fe, *etc.*) have been studied as substitutes for Zn. A library of CXTS compounds was successfully fabricated using spray pyrolysis. While Cu_2MnSnS_4, Cu_2BaSnS_4, and Cu_2SrSnS_4 demonstrated good device performances, forming pure phases for some compounds was difficult.[13] Efforts have also been made to alloy a high amount of Ge for CZGSe, leading to a 7.6% efficiency and a further 8.5% after surface treatment and heat treatment on a complete device

---

[a] School of Materials Science and Engineering, Nanyang Technological University, Singapore 639798, Singapore. E-mail: lydiawong@ntu.edu.sg
[b] Campus for Research Excellence and Technological Enterprise (CREATE), Singapore 138602, Singapore
[c] Davidson School of Chemical Engineering, Purdue University, West Lafayette, Indiana 47907, USA
[d] Solar Energy Materials and Systems Group, Catalonia Institute for Energy Research (IREC), Jardins de les Dones de Negre 1, 08930 Sant Adrià de Besòs, Barcelona, Spain
[e] Photovoltaic Lab – Micro and Nano Technologies Group (MNT), Electronic Engineering Department, EEBE, Universitat Politècnica de Catalunya (UPC), Av Eduard Maristany 10-14, Barcelona 08019, Catalonia, Spain
[f] Barcelona Center for Multiscale Science & Engineering, Universitat Politècnica de Catalunya (UPC), Av Eduard Maristany 10-14, Barcelona 08019, Catalonia, Spain
[g] Energy Research Institute @ NTU (ERI@N), Nanyang Technological University, Singapore 637553, Singapore

† Electronic supplementary information (ESI) available. See DOI: https://doi.org/10.1039/d3ta04529c

(including MgF_2 anti-reflection coating layer).[14,15] Among all these cations, Cu_2CdSnS_4 has the highest device performance so far.

The favorable material properties of Cu_2CdSnS_4 make it a promising candidate for further development as one of the emerging thin film solar cells. The Cu_2CdSnS_4 solar cell has shown remarkable device performance, starting with an efficiency of 7.96%, which recently has been improved to 10.1%, placing it among the highest reported efficiency of emerging kesterite-inspired solar cell devices and close to the 11.0% certified record efficiency for pure sulfide Cu_2ZnSnS_4.[16–19] The suppressed $2Cu_{Cd} + Sn_{Cd}$ defect formation, due to its higher formation energy compared to $2Cu_{Zn} + Sn_{Zn}$ in Cu_2ZnSnS_4, is attributed to the promising properties of this material. Both defect complexes act as deep electron traps[3,20] and contribute to the increase of bandgap fluctuation and nonradiative recombination. Cu-Poor condition, commonly employed in kesterite solar cells, further suppressed the $2Cu_{Cd} + Sn_{Cd}$ defect.[16] This non-stoichiometric condition and optimized sulfurization configuration were also crucial for the recent device efficiency improvement.[17] While the current achievements for Cu_2CdSnS_4 solar cells are encouraging, additional strategies such as doping and alloying could be important to understand this compound better.

The cation substitution (and doping) strategies in Cu_2CdSnS_4 have yet to be thoroughly studied. While the beneficial roles of Ag have been observed in partially Cd-substituted Cu_2ZnSnS_4 compounds, its impact on the material and photovoltaic properties of Cu_2CdSnS_4 remains unexplored.[9,21] Additionally, the absorption coefficient of Ag_2CdSnS_4 has been calculated to be suitable for a solar cell.[22] The larger Ag^+ ionic radii (1.00 Å) compared to Cu^+ (0.60 Å) suggest that substituting Cu to Ag could further reduce $2Cu_{Cd} + Sn_{Cd}$ defects. Other theoretical works highlighted that as the difference in ionic radii size of Ag–Cd is not as high as Ag–Zn (Ag^+ to Cd^{2+} is 28% larger, while Ag^+ to Zn^{2+} is 66% larger), Ag_2CdSnS_4 might not be as disorder-resistant as compared to Ag_2ZnSnS_4.[23,24] This work aims to investigate the effect of Ag substitution for Cu_2CdSnS_4 by comparing phase distribution, film morphology, and device performance as part of its structural, optoelectronic, and photovoltaic properties. The small addition of Ag in Cu_2CdSnS_4 improved device performance to 7.72% compared to 6.87% reference, but the improvement is limited by the presence of mixed phases at higher Ag concentrations. This limitation will be explored by studying the transformation from Cu_2CdSnS_4 to Ag_2CdSnS_4, correlating the transition with the evolution of the device performance. Finally, the fully-substituted Ag_2CdSnS_4 induced doping type inversion, high carrier mobility, and exhibits a sharp absorption onset.

Results and discussion

In this study, we monotonically modify the concentration of Ag by depositing the precursor solutions using spin-coating, starting from pure Cu_2CdSnS_4 (Ag/[Ag + Cu] = 0%) to Ag_2CdSnS_4 (Ag/[Ag + Cu] = 100%). The selection of 5% and 10% Ag was based on the optimal device efficiency observed in previous Cu_2ZnSnS_4 devices.[25–28] The films for all Ag concentrations were characterized for their structural and optoelectronic properties, while only selected concentrations were made into full devices.

Structural properties of $(Cu_{1-x}Ag_x)_2CdSnS_4$

The diffractograms (Fig. 1a) obtained from as-fabricated Cu_2CdSnS_4 film fit the reported database and showed major peaks at 28° and 47° associated with (112) and (204) of the Cu_2CdSnS_4 stannite plane (JCPDS No. 29-0537). The magnified XRD spectra in the range of $2\theta = 23–30°$ is shown in Fig. 1b, highlighting the transition from tetragonal Cu_2CdSnS_4 to orthorhombic Ag_2CdSnS_4 phase. In the range of 0–20% Ag substitution, there is a subtle shift to a lower diffraction angle at the (112) peak due to the successful incorporation of larger Ag ions.[29] The slight 40° diffraction angle is from the Mo substrate and thus is used as a reference for the peak shifting for other Ag concentrations. It is observed that the transition from Cu_2CdSnS_4 towards mixed phases with Ag_2CdSnS_4 starts at 30% Ag substitution. Starting at this concentration up to 80% Ag, it can also be observed that the film quality is deteriorating as the main peak intensity is relatively low compared to the Mo peak as substrate. The shifting trend of the (112) peak of Cu_2CdSnS_4 continued to higher Ag concentrations too. The primary peaks at 25.06°, 26.54°, and 28.48° associated with (011), (200), and (111) of the Ag_2CdSnS_4 planes are observed, respectively.

To identify the presence of secondary phases, Raman measurement for all films were conducted as shown in Fig. 1c. Under 532 nm excitation wavelength, the Cu_2CdSnS_4 film exhibits its characteristics symmetry modes at 332 and 283 cm^{-1}, similar to previously reported Raman data.[16,17] The appearance of these two peaks dominates up to 20% Ag. Note that the CdS secondary phase can also be identified in the spectra, especially at the 30–80% Ag films, where the film quality seems to deteriorate. On the other hand, no Cu_2SnS_3 secondary phase (290 and 350 cm^{-1}) is detected on all films. At the higher amount of Ag (≥60%), the main peak at 332 cm^{-1} shifts to a higher wavenumber value, and the appearance of a shoulder peak at 367 cm^{-1} suggests a change in the phase from the stannite Cu_2CdSnS_4 to orthorhombic Ag_2CdSnS_4. Although to our knowledge Raman studies about Ag_2CdSnS_4 have not been reported, K. Pietak *et al.* presented in their study of Ag_2ZnSnS_4 similar results regarding their Raman measurements with the appearance of an intense peak at 341 cm^{-1} as well as an additional peak at 370 cm^{-1}.[30] In addition to our XRD, it seems that the observed Raman peaks phase belongs to orthorhombic Ag_2CdSnS_4, the first time it has been reported in the literature.

The transition between Cu_2CdSnS_4 into Ag_2CdSnS_4 was also quantitively studied by Rietveld refinement of the XRD spectra. All films have been refined to their tetragonal unit cells for Cu_2CdSnS_4, orthorhombic for Ag_2CdSnS_4, and both for the partial Cu–Ag substitution. The value of R_{bragg} evaluates how well each phase fits with the model, the lower, the better. The goodness of fit (GOF), representing the closeness of the refinement model to the actual measured data with one as the ideal value, is used to determine the refinement model quality. The GOF equation is shown below,

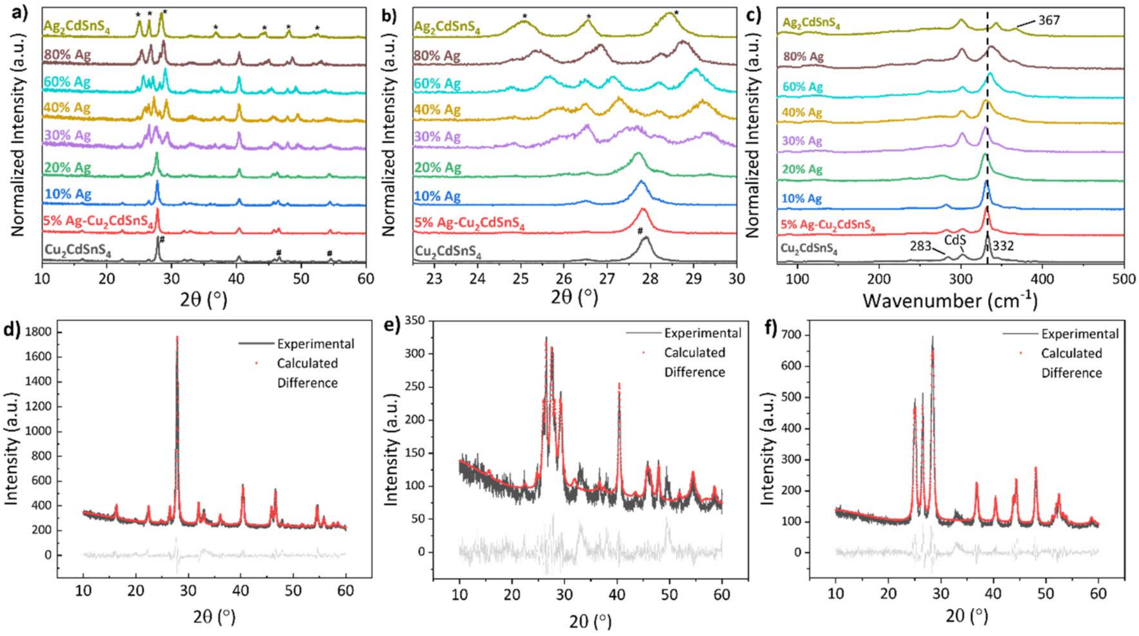

Fig. 1 (a) X-ray diffraction (XRD) pattern and (c) Raman spectra of Cu_2CdSnS_4 film with various Ag content and Ag_2CdSnS_4 film. (b) Magnified XRD view on 23–30° diffraction angle near (112) peak of Cu_2CdSnS_4; the intensities in (a–c) are normalized, % Ag refers to the concentration ratio of Ag/Ag + Cu. (d) Refinement plot for Cu_2CdSnS_4 sample, (e) 30% Ag of $(Cu_{1-x}Ag_x)_2CdSnS_4$ sample, and (f) Ag_2CdSnS_4 sample.

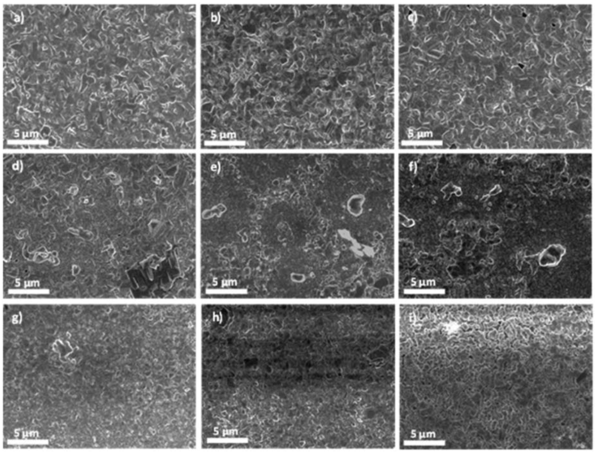

Fig. 2 Surface SEM images for (a) Cu_2CdSnS_4 and additional Ag content of (b) 5%, (c) 10%, (d) 20%, (e) 30%, (f) 40%, (g) 60%, (h) 80%, and for (i) Ag_2CdSnS_4.

$$\mathrm{GOF} = \chi^2 = \left[\frac{R_{\mathrm{wp}}}{R_{\mathrm{exp}}}\right]^2$$

where R_{wp} is the residual weighing the fitting of the model to the peak intensities, and R_{exp} is the residual for the experimental value evaluation.[31]

The refinement for pure Cu_2CdSnS_4 sample can be closely fitted ($R_{\mathrm{bragg}} = 3.79$; GOF = 1.53) to the calculated tetragonal unit cells, as shown in Fig. 1d. This fitting case still applies after adding 5% up to 20% Ag (Fig. S1†). At 30% Ag, the experimental data shown in Fig. 1e cannot be reasonably fitted to tetragonal Cu_2CdSnS_4 ($R_{\mathrm{bragg}} = 5.27$) or orthorhombic Ag_2CdSnS_4 ($R_{\mathrm{bragg}} = 9.66$). Finally, the 80% Ag ($R_{\mathrm{bragg}} = 2.72$; GOF = 1.47) and pure Ag_2CdSnS_4 ($R_{\mathrm{bragg}} = 2.95$; GOF = 1.46) data have a close fit to the calculated orthorhombic unit cells, as shown in Fig. 1f and S1.†

Following, the study on film morphology (Fig. 2) is carried out. Pure Cu_2CdSnS_4 and the Ag-alloyed films have large and compact grains with up to a 10% Ag concentration ratio. Meanwhile, the grains become smaller and less uniform between 20% and 40% Ag. While the presence of grain boundaries could be benign for high efficiency $Cu(In,Ga)Se_2$ thin film solar cells due to the effective passivation by alkali,[32,33] in general for polycrystalline material, such as the more closely related Cu_2ZnSnS_4, grain boundaries may introduce additional deep level states within the energy bandgap acting as effective recombination centre.[34,35] The grains become more uniform as the Ag content increases to 60%. Finally, the Ag_2CdSnS_4 film has uniform grains, albeit smaller than the Cu_2CdSnS_4 film. This means the uniform grains that could benefit a solar cell device can be obtained from pure Cu_2CdSnS_4 and Ag_2CdSnS_4 film, as well as the 5% Ag.

The elemental ratios of the films were measured by EDS, as shown in Table S1.† All the films have non-stoichiometric Cu-poor and Cd-rich compositions similar to the as-prepared solutions. The Ag concentration in each variation is in good agreement with the prepared amount. A line scan was conducted for 5% and 30% Ag films to check the elemental distribution of the film. Ag is distributed uniformly throughout both films, similar to other cations, as shown in Fig. S2.† Thus, there is no Ag distribution grading for both the small and mixed phases concentrations.

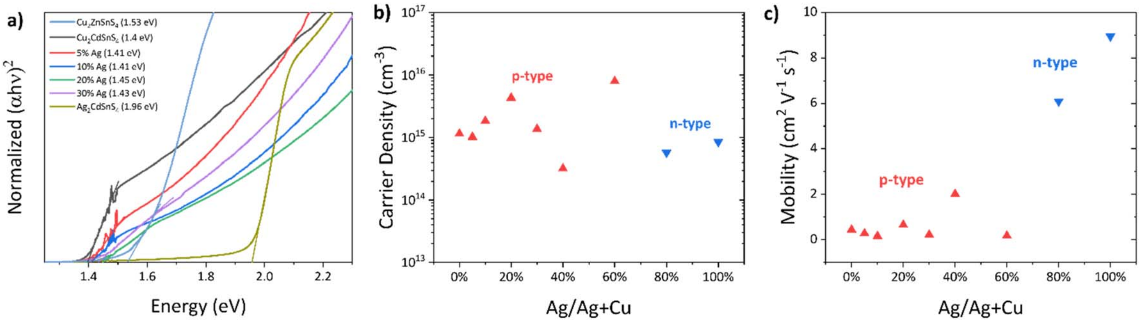

Fig. 3 (a) Tauc plot of $(\alpha h\nu)^2$ as a function of $h\nu$ for Cu_2ZnSnS_4 and $(Cu_{1-x}Ag_x)_2CdSnS_4$ films; (b) apparent carrier concentration and (c) mobility extracted from Hall film measurement for $(Cu_{1-x}Ag_x)_2CdSnS_4$ with various Ag concentrations.

Optoelectronic properties of $(Cu_{1-x}Ag_x)_2CdSnS_4$

UV-Vis was conducted for all concentrations to understand further the optoelectronic properties of the $(Cu_{1-x}Ag_x)_2CdSnS_4$ films. The increased bandgap for $(Cu_{1-x}Ag_x)_2CdSnS_4$ in Fig. 3a and S3† can be attributed to the higher incorporation of Ag, as demonstrated by the peaks shifting observed from XRD. The absorption edge for pure Cu_2CdSnS_4 and small concentrations of Ag up to 10% are quite sharp, indicating their better light absorption ability, while it is less so for 20% Ag and 30% Ag. At 30% Ag, the mixed phases clearly contributed to the less sharp absorption edge. This observation is the same for higher Ag concentrations, but for pure Ag_2CdSnS_4, a clear, sharp absorption edge comparable to Cu_2CdSnS_4 and Cu_2ZnSnS_4 can be obtained with an extracted bandgap of 1.93 eV.

Hall measurement is then conducted for all concentrations of the $(Cu_{1-x}Ag_x)_2CdSnS_4$ films. The apparent carrier concentration for Cu_2CdSnS_4 is 2.7×10^{15} cm^{-3} with carrier mobility of 0.44 cm^2 V^{-1} s^{-1}. The presence of mixed phases from 30% to 80% Ag could affect the values of their carrier density, as there is no clear correlation between carrier concentration and mobility values to the Ag concentrations, as observed in Fig. 3. Interestingly, the doping type changes between p-type for Cu_2CdSnS_4 into n-type for Ag_2CdSnS_4. The high formation energy of its acceptor defects could be the reason for this transition, as similarly observed in Ag_2ZnSnS_4 and $Ag_2ZnSnSe_4$.[11,12]

The highest peaks obtained from photoluminescence spectra in Fig. S4a† do not represent the bandgaps of all the samples. However, secondary peaks around 1.35 eV close to each respective bandgap value of 5% and 10% Ag films were observed, indicating fewer defects or improved quality after small doping of Ag. The main peaks for higher concentrations of Ag (30%, 60%, and pure Ag_2CdSnS_4) were all blue-shifted corresponding to their higher bandgaps.

Photovoltaic properties of $(Cu_{1-x}Ag_x)_2CdSnS_4$

The complete device configuration is SLG/Mo/$(Cu_{1-x}Ag_x)_2$-$CdSnS_4$/CdS/ITO without anti-reflection coating. *I–V* measurements were conducted on at least ten devices for each Ag concentration to obtain statistical representation. The photovoltaic parameters for the devices up to 60% Ag are presented in Fig. 4. Between 0% to 10% Ag, there is no significant improvement in FF and V_{OC}. The performance starts to drop at 20% Ag concentration, accompanied by a drop in J_{SC} and FF, which can be related to the presence of non-uniform grains and voids on the film. The presence of mixed phases between 30% and 40% Ag is well-reflected in the device performance. While for 30% Ag, the V_{OC} is comparable with lesser Ag concentration, at 40%, the V_{OC} drops significantly.

Both 30% and 40% of Ag devices have poor FF and J_{SC}. The presence of pinholes might be responsible for the poor V_{OC} and FF at those concentrations. At the same time, the J_{SC} also suffers from carrier recombination at the grain boundaries due to poor grain growth on top of the increasing bandgap. The devices have very poor performance when Ag content is higher than Cu at 60%, which could be attributed to the much higher bandgap affecting the band alignment with the CdS layer. Moreover, despite improved morphology conditions at 80% and 100% Ag, an alternative device configuration might be necessary to conform to the n-type majority carriers' condition, as observed in Fig. 3. Lastly, we did not obtain a working Ag_2CdSnS_4 device because the remaining pure phase is n-type at this concentration.

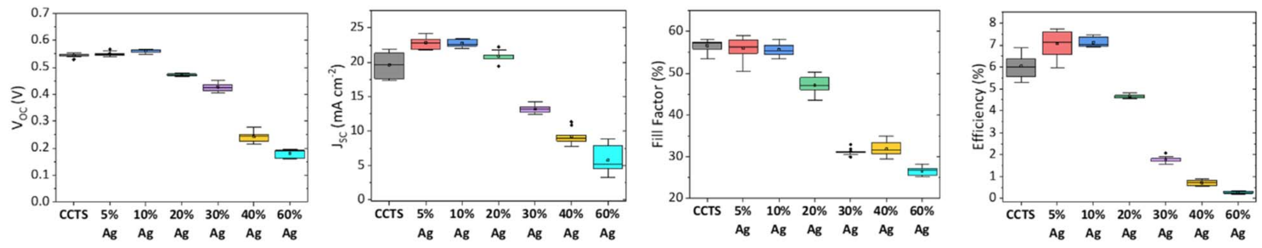

Fig. 4 Device parameters for Cu_2CdSnS_4 with various Ag concentrations. All boxplots represent ten devices each.

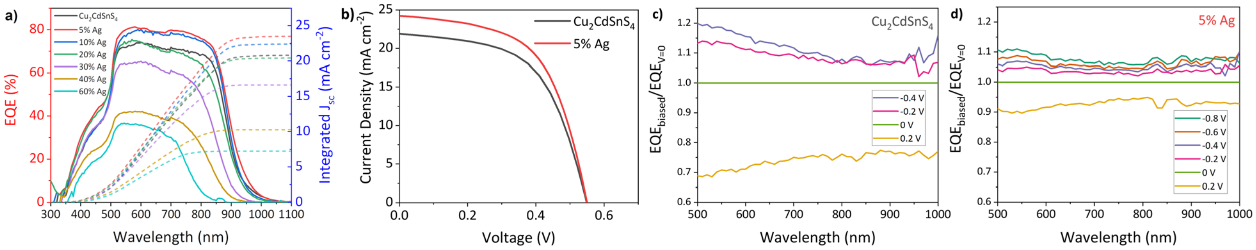

Fig. 5 (a) External quantum efficiency (EQE) curves (left axis) and their integrated J_{SC} (right axis-dashes) for Cu_2CdSnS_4 with various Ag concentrations, (b) I–V curves for the best Cu_2CdSnS_4 and 5% Ag device. Voltage-biased EQE curves for (c) Cu_2CdSnS_4 and (d) 5% Ag device normalized to the unbiased EQE values.

Table 1 Photovoltaic parameters of the best Cu_2CdSnS_4 and 5% Ag device

Device	V_{OC} [mV]	J_{SC} [mA cm^{-2}]	FF [%]	η [%]	E_g [eV]	n	J_{01} [$\times10^{-6}$ A cm^{-2}]	R_s [Ω cm^2]	G_{sh} [mS cm^{-2}]
Cu_2CdSnS_4	549	21.89	57.16	6.87	1.39	2.35	2.23	2.55	3.93
5% Ag	550	24.23	57.89	7.72	1.41	2.64	6.64	1.63	3.79

The External Quantum Efficiency (EQE) for the best-performing devices up to 60% Ag concentration is shown in Fig. 5a. Poor EQE results were obtained for Ag concentrations above 60%. The J_{SC} improvement for 5% and 10% Ag devices is well-reflected by each device's higher EQE values, which is translated to the higher integrated J_{SC} values. For 5% Ag, the EQE increases throughout the whole wavelength. This improvement can be attributed to the reduced recombination at the bulk of Cu_2CdSnS_4 due to small Ag content doping.[36] Similar improvement is observed from the 10% Ag, but there is a reduction at the lower wavelength, probably due to parasitic absorption of the top layers from CdS/ITO.[37] The higher Ag contents are consistent between J_{SC} values and the EQE. At higher concentrations, the bandgap increases to 1.63 eV for 60% Ag. This increasing trend is also obtained from the extracted bandgap values from the absorption spectra in Fig. S3.† Moreover, this is also consistent with the experimentally observed 1.93 eV bandgap for pure Ag_2CdSnS_4.[38]

The improvement for the best device with 5% Ag mainly comes from slightly higher J_{SC} and Fill Factor (FF) compared to the pure Cu_2CdSnS_4 devices, as observed in Table 1 and Fig. 5b. The better FF for the 5% Ag device is in good agreement with its lower R_s and G_{sh} value. The same J_{SC} improvement for the small amount of Ag was also observed in CZTS devices with a high Cd substitution concentration. It was attributed to larger grain sizes and enhanced depletion width.[9]

To further understand the reason for the improved performance of the 5% Ag device, we performed a C–V measurement. Comparing the pure Cu_2CdSnS_4 and 5% Ag devices, as shown in Fig. S5,† the extracted carrier concentration for these devices does not significantly change, as similarly observed from Hall measurement (Table S2†). The amount of Ag might be too small to significantly affect the carrier density. Nevertheless, the 5% Ag device shows a slight improvement in its depletion width, leading to a better carrier collection, as reflected by its superior EQE. We also performed EQE measurements under positive and negative voltage bias for the two devices, as shown in Fig. 5c and d. The $EQE_{biased}/EQE_{V=0}$ ratio indicates severe interface recombination in Cu_2CdSnS_4. In particular, the large deviation of this ratio from the ideal value of 1 and the corresponding slope of the dependence of this ratio on wavelength suggests the presence of interface recombination.[36] Adding 5% Ag to Cu_2CdSnS_4 brings this ratio closer to 1, suggesting that interface recombination in these devices is suppressed to some extent. The 5% Ag device performance improvement can be mainly attributed to this reason and the better film quality as demonstrated by the presence of a PL peak at the energy level close to its bandgap value.

The EQE spectrum onset for Cu_2CdSnS_4 and 5% Ag devices was further analyzed by evaluating its derivative $d(-\ln(1 - EQE))/dE$ as presented in Fig. S6† referring to previous methods in the literature.[39,40] According to Mattheis *et al.*,[39] the standard deviation of the Gaussian fitting of the derivative $d(-\ln(1 - EQE))/dE$ represents the amplitude of bandgap fluctuations (σ_{E_g}). For the 5% Ag device, the σ_{E_g} value of 56 meV is not far from the σ_{E_g} value of the Cu_2CdSnS_4 device (58 meV). However, these values are much smaller than our similarly processed Cu_2ZnSnS_4 solar cell device (116 meV) and comparable to the σ_{E_g} value of the current 13.8% record efficiency $Cu_2ZnSn(S,Se)_4$ (CZTSSe) solar cell device, which is about 52 meV.[41] As the degree of bandgap fluctuations has been associated with the $2Cu_{Cd} + Sn_{Cd}$ (or $2Cu_{Zn} + Sn_{Zn}$) deep defects,[3,16,42] the small σ_{E_g} values of Cu_2CdSnS_4 and 5% Ag devices indicate the suppression of the associated deep defects. A combination of this work and the use of Sn^{4+} precursors (used in the 13.8% CZTSSe device and currently regarded as essential for high-efficiency CZTSSe solar cells) might give better CCTS device performance in future studies.

Conclusions

In this work, we have investigated Ag substitution on Cu_2CdSnS_4 and monotonically studied its transition. The phase transition from tetragonal Cu_2CdSnS_4 to orthorhombic

Ag_2CdSnS_4 starts at 30% Ag concentration, as observed from the XRD spectra. Despite the bigger ionic radii size (Ag 1.00 Å *vs.* Cu 0.60 Å, Cd 0.78 Å), higher Ag concentrations do not effectively translate into better photovoltaic performance. This is demonstrated by its poor crystal quality, optoelectronic properties, and possible carrier-type changes. However, the n-type nature of the fully-substituted Ag_2CdSnS_4 might require a different device configuration and further optimization to obtain a working solar cell device. On the other hand, small amounts of Ag concentrations of up to 10% have improved device performance compared to pure Cu_2CdSnS_4. The 5% Ag device has the best performance of 7.72%, which is attributed to its better film quality and superior interface properties, leading to its higher J_{SC} compared to the pure Cu_2CdSnS_4.

Author contributions

A. I. fabricated the $(Cu_{1-x}Ag_x)_2CdSnS_4$ thin films, conducted XRD and its Rietveld analysis, carried out SEM-EDS, UV-Vis, Hall measurement and solar cell device characterization, and analyzed the raw data. S. L. helped with the analysis of solar cell device characterization and Hall measurement results. J. M. R. T. contributed suggestions on the synthesis. R. S. performed the PL measurements, EQE-V, and helped with the analysis of the results (supervised by R. A.). A. G. M. conducted Raman measurement and helped with the discussion of the result (supervised by E. S.). S. H. contributed suggestions on EQE-V data. L. H. W. supervised the work.

Conflicts of interest

There are no conflicts to declare.

Acknowledgements

The authors would like to acknowledge the funding support from the CREATE Programme under the Campus for Research Excellence and Technological Enterprise (CREATE), which is supported by the National Research Foundation, Prime Minister's Office, Singapore, and the Ministry of Education (MOE) Tier 2 Project (MOE-T2EP50120-0008). Also, we would like to acknowledge the Facility for Analysis, Characterisation, Testing and Simulation (FACTS), Nanyang Technological University, Singapore, for use of their X-ray facilities.

References

1 S. Giraldo, Z. Jehl, M. Placidi, V. Izquierdo-Roca, A. Pérez-Rodríguez and E. Saucedo, Progress and Perspectives of Thin Film Kesterite Photovoltaic Technology: A Critical Review, *Adv. Mater.*, 2019, **31**, 1–18.

2 S. Hadke, M. Huang, C. Chen, Y. F. Tay, S. Chen, J. Tang and L. Wong, Emerging Chalcogenide Thin Films for Solar Energy Harvesting Devices, *Chem. Rev.*, 2022, **122**, 10170–10265.

3 S. Chen, A. Walsh, X. G. Gong and S. H. Wei, Classification of lattice defects in the kesterite Cu_2ZnSnS_4 and $Cu_2ZnSnSe_4$ earth-abundant solar cell absorbers, *Adv. Mater.*, 2013, **25**, 1522–1539.

4 J. Fu, Q. Tian, Z. Zhou, D. Kou, Y. Meng, W. Zhou and S. Wu, Improving the Performance of Solution-Processed $Cu_2ZnSn(S,Se)_4$ Photovoltaic Materials by Cd^{2+} Substitution, *Chem. Mater.*, 2016, **28**, 5821–5828.

5 R. Sun, D. Zhuang, M. Zhao, Q. Gong, M. Scarpulla, Y. Wei, G. Ren and Y. Wu, Beyond 11% efficient $Cu_2ZnSn(Se,S)_4$ thin film solar cells by cadmium alloying, *Sol. Energy Mater. Sol. Cells*, 2018, **174**, 494–498.

6 C. Yan, K. Sun, J. Huang, S. Johnston, F. Liu, B. P. Veettil, K. Sun, A. Pu, F. Zhou, J. A. Stride, M. A. Green and X. Hao, Beyond 11% Efficient Sulfide Kesterite $Cu_2Zn_xCd_{1-x}SnS_4$ Solar Cell: Effects of Cadmium Alloying, *ACS Energy Lett.*, 2017, **2**, 930–936.

7 Z. Su, J. M. R. Tan, X. Li, X. Zeng, S. K. Batabyal and L. H. Wong, Cation Substitution of Solution-Processed Cu_2ZnSnS_4 Thin Film Solar Cell with over 9% Efficiency, *Adv. Energy Mater.*, 2015, **5**, 1500682.

8 A. Guchhait, Z. Su, Y. F. Tay, S. Shukla, W. Li, S. W. Leow, J. M. R. Tan, S. Lie, O. Gunawan and L. H. Wong, Enhancement of Open-Circuit Voltage of Solution-Processed Cu_2ZnSnS_4 Solar Cells with 7.2% Efficiency by Incorporation of Silver, *ACS Energy Lett.*, 2016, **1**, 1256–1261.

9 S. H. Hadke, S. Levcenko, S. Lie, C. J. Hages, J. A. Márquez, T. Unold and L. H. Wong, Synergistic Effects of Double Cation Substitution in Solution-Processed CZTS Solar Cells with over 10% Efficiency, *Adv. Energy Mater.*, 2018, **8**, 1802540.

10 C. Ma, H. Guo, K. Zhang, N. Yuan and J. Ding, Fabrication of p-type kesterite Ag_2ZnSnS_4 thin films with a high hole mobility, *Mater. Lett.*, 2017, **186**, 390–393.

11 T. Gershon, K. Sardashti, O. Gunawan, R. Mankad, S. Singh, Y. S. Lee, J. A. Ott, A. Kummel and R. Haight, Photovoltaic Device with over 5% Efficiency Based on an n-Type $Ag_2ZnSnSe_4$ Absorber, *Adv. Energy Mater.*, 2016, **6**, 1601182.

12 H. Guo, C. Ma, K. Zhang, X. Jia, Y. Li, N. Yuan and J. Ding, The fabrication of Cd-free Cu_2ZnSnS_4-Ag_2ZnSnS_4 heterojunction photovoltaic devices, *Sol. Energy Mater. Sol. Cells*, 2018, **178**, 146–153.

13 S. Lie, M. Guc, V. Tunuguntla, V. Izquierdo-Roca, S. Siebentritt and L. H. Wong, Comprehensive physicochemical and photovoltaic analysis of different Zn substitutes (Mn, Mg, Fe, Ni, Co, Ba, Sr) in CZTS-inspired thin film solar cells, *J. Mater. Chem. A*, 2022, 9137–9149.

14 L. Choubrac, G. Brammertz, N. Barreau, L. Arzel, S. Harel, M. Meuris and B. Vermang, 7.6% CZGSe Solar Cells Thanks to Optimized CdS Chemical Bath Deposition, *Phys. Status Solidi*, 2018, **215**, 1800043.

15 L. Choubrac, M. Bär, X. Kozina, R. Félix, R. G. Wilks, G. Brammertz, S. Levcenko, L. Arzel, N. Barreau, S. Harel, M. Meuris and B. Vermang, Sn Substitution by Ge: Strategies to Overcome the Open-Circuit Voltage Deficit of Kesterite Solar Cells, *ACS Appl. Energy Mater.*, 2020, **3**, 5830–5839.

16 S. Hadke, S. Levcenko, G. Sai Gautam, C. J. Hages, J. A. Márquez, V. Izquierdo-Roca, E. A. Carter, T. Unold

and L. H. Wong, Suppressed Deep Traps and Bandgap Fluctuations in Cu_2CdSnS_4 Solar Cells with ≈8% Efficiency, *Adv. Energy Mater.*, 2019, **9**, 1902509.

17 P. Fan, J. Lin, J. Hu, Z. Yu, Y. Zhao, S. Chen, Z. Zheng, J. Luo, G. Liang and Z. Su, Over 10% Efficient Cu_2CdSnS_4 Solar Cells Fabricated from Optimized Sulfurization, *Adv. Funct. Mater.*, 2022, **32**, 2207470.

18 Y. E. Romanyuk, S. G. Haass, S. Giraldo, M. Placidi, D. Tiwari, D. J. Fermin, X. Hao, H. Xin, T. Schnabel, M. Kauk-Kuusik, P. Pistor, S. Lie and L. H. Wong, Doping and alloying of kesterites, *JPhys Energy*, 2019, **1**, 044004.

19 C. Yan, J. Huang, K. Sun, S. Johnston, Y. Zhang, H. Sun, A. Pu, M. He, F. Liu, K. Eder, L. Yang, J. M. Cairney, N. J. Ekins-Daukes, Z. Hameiri, J. A. Stride, S. Chen, M. A. Green and X. Hao, Cu_2ZnSnS_4 solar cells with over 10% power conversion efficiency enabled by heterojunction heat treatment, *Nat. Energy*, 2018, **3**, 764–772.

20 L. Meng, Y. Li, B. Yao, Z. H. Ding, G. Yang, R. J. Liu, R. Deng and L. Liu, Mechanism of effect of intrinsic defects on electrical and optical properties of Cu_2CdSnS_4: An experimental and first-principles study, *J. Phys. D Appl. Phys.*, 2015, **48**, 445105.

21 K. Timmo, M. Altosaar, M. Pilvet, V. Mikli, M. Grossberg, M. Danilson, T. Raadik, R. Josepson, J. Krustok and M. Kauk-Kuusik, The effect of Ag alloying of $Cu_2(Zn,Cd)SnS_4$ on the monograin powder properties and solar cell performance, *J. Mater. Chem. A*, 2019, **7**, 24281–24291.

22 S. Saidi, S. Zriouel, L. B. Drissi and M. Maaroufi, First principles study of electronic and optical properties of Ag_2CdSnS_4 chalcogenides for photovoltaic applications, *Comput. Mater. Sci.*, 2018, **152**, 291–299.

23 T. Küllmey, J. Hein, E. M. Heppke, I. Efthimiopoulos and B. Paulus, High-Pressure Behavior and Disorder for Ag_2ZnSnS_4 and Ag_2CdSnS_4, *ACS Omega*, 2021, **6**, 27387–27395.

24 E. M. Heppke, S. Berendts and M. Lerch, Crystal structure of mechanochemically synthesized Ag_2 $CdSnS_4$, *Z. Naturforsch., B*, 2020, **75**, 393–402.

25 Y.-F. Qi, D.-X. Kou, W.-H. Zhou, Z.-J. Zhou, Q.-W. Tian, Y.-N. Meng, X.-S. Liu, Z.-L. Du and S.-X. Wu, Engineering of interface band bending and defects elimination via a Ag-graded active layer for efficient $(Cu,Ag)_2ZnSn(S,Se)_4$ solar cells, *Energy Environ. Sci.*, 2017, **10**, 2401–2410.

26 W.-C. Huang, S.-Y. Wei, C.-H. Cai, W.-H. Ho and C.-H. Lai, The role of Ag in aqueous solution processed $(Ag,Cu)_2ZnSn(S,Se)_4$ kesterite solar cells: antisite defect elimination and importance of Na passivation, *J. Mater. Chem. A*, 2018, **6**, 15170–15181.

27 Y. Qi, Y. Liu, D. Kou, W. Zhou, Z. Zhou, Q. Tian, S. Yuan, Y. Meng and S. Wu, Enhancing Grain Growth for Efficient Solution-Processed $(Cu,Ag)_2ZnSn(S,Se)_4$ Solar Cells Based on Acetate Precursor, *ACS Appl. Mater. Interfaces*, 2020, **12**, 14213–14223.

28 Y. Qi, X. Zhao, Y. Liu, D. Kou, W. Zhou, Z. Zhou, S. Yuan, Y. Meng and S. Wu, Synergistic effect of Mn on bandgap fluctuations and surface electrical characteristics in Ag-based $Cu_2ZnSn(S,Se)_4$ solar cells, *J. Mater. Chem. A*, 2021, **9**, 2292–2300.

29 R. D. Shannon, Revised effective ionic radii and systematic studies of interatomic distances in halides and chalcogenides, *Acta Crystallogr., Sect. A*, 1976, **32**, 751–767.

30 K. Pietak, C. Jastrzebski, K. Zberecki, D. J. Jastrzebski, W. Paszkowicz and S. Podsiadlo, Synthesis and structural characterization of Ag_2ZnSnS_4 crystals, *J. Solid State Chem.*, 2020, **290**, 2–7.

31 R. A. Young, *The Rietveld Method*, Oxford University Press, 1995.

32 C. S. Jiang, R. Noufi, J. A. AbuShama, K. Ramanathan, H. R. Moutinho, J. Pankow and M. M. Al-Jassim, Local built-in potential on grain boundary of $Cu(In,Ga)Se_2$ thin films, *Appl. Phys. Lett.*, 2004, **84**, 3477–3479.

33 N. Nicoara, R. Manaligod, P. Jackson, D. Hariskos, W. Witte, G. Sozzi, R. Menozzi and S. Sadewasser, Direct evidence for grain boundary passivation in $Cu(In,Ga)Se_2$ solar cells through alkali-fluoride post-deposition treatments, *Nat. Commun.*, 2019, **10**, 1–8.

34 J. Li, D. B. Mitzi and V. B. Shenoy, Structure and electronic properties of grain boundaries in earth-abundant photovoltaic absorber $Cu_2ZnSnSe_4$, *ACS Nano*, 2011, **5**, 8613–8619.

35 J. Li, J. Huang, F. Ma, H. Sun, J. Cong, K. Privat, R. F. Webster, S. Cheong, Y. Yao, R. L. Chin, X. Yuan, M. He, K. Sun, H. Li, Y. Mai, Z. Hameiri, N. J. Ekins-Daukes, R. D. Tilley, T. Unold, M. A. Green and X. Hao, Unveiling microscopic carrier loss mechanisms in 12% efficient $Cu_2ZnSnSe_4$ solar cells, *Nat. Energy*, 2022, **7**, 754–764.

36 Y. F. Tay, S. S. Hadke, M. Zhang, N. Lim, S. Y. Chiam and L. H. Wong, Improving the interfacial properties of CZTS photocathodes by Ag substitution, *J. Mater. Chem. A*, 2020, **8**, 8862–8867.

37 W. Wang, M. T. Winkler, O. Gunawan, T. Gokmen, T. K. Todorov, Y. Zhu and D. B. Mitzi, Device characteristics of CZTSSe thin-film solar cells with 12.6% efficiency, *Adv. Energy Mater.*, 2014, **4**, 1–5.

38 G. E. Davydyuk, G. L. Myronchuk, I. V. Kityk, S. P. Danyl'Chuk, V. V. Bozhko and O. V. Parasyuk, Ag_2CdSnS_4 single crystals as promising materials for optoelectronic, *Opt. Mater.*, 2011, **33**, 1302–1306.

39 J. Mattheis, U. Rau and J. H. Werner, Light absorption and emission in semiconductors with band gap fluctuations-A study on $Cu(In,Ga)Se_2$ thin films, *J. Appl. Phys.*, 2007, **101**, 113519.

40 U. Rau, B. Blank, T. C. M. Müller and T. Kirchartz, Efficiency Potential of Photovoltaic Materials and Devices Unveiled by Detailed-Balance Analysis, *Phys. Rev. Appl.*, 2017, **7**, 1–9.

41 J. Zhou, X. Xu, H. Wu, J. Wang, L. Lou, K. Yin, Y. Gong, J. Shi, Y. Luo, D. Li, H. Xin and Q. Meng, Control of the phase evolution of kesterite by tuning of the selenium partial pressure for solar cells with 13.8% certified efficiency, *Nat. Energy*, 2023, **8**, 526–535.

42 G. Rey, G. Larramona, S. Bourdais, C. Choné, B. Delatouche, A. Jacob, G. Dennler and S. Siebentritt, On the origin of band-tails in kesterite, *Sol. Energy Mater. Sol. Cells*, 2018, **179**, 142–151.